Unitarity constraints and collider searches for dark photons

Yasaman Hosseini and Mojtaba Mohammadi Najafabadi
School of Particles and Accelerators, Institute for Research in Fundamental Sciences (IPM), P.O. Box 19395-5531, Tehran, Iran

(Received 24 February 2022; accepted 18 July 2022; published 28 July 2022)

Dark photons are predicted by various new physics models and are being intensively studied in a variety of experiments. In the first part of this paper, we obtain partial wave unitarity constraints on the dark photon parameter space from the allowed $VV \to VV$ scattering processes in the limit of large center-of-mass energy, where $V = W, Z$. In the second part of the paper, searches are performed using the expected differential rates with a realistic detector simulation including a comprehensive set of background processes on dilepton and dilepton plus a photon events at the High Luminosity LHC. In these searches, sensitive differential distributions are used in an optimized way to determine the sensitivity to dark photon parameter space. It is shown that remarkable sensitivity to the dark photon model is achieved, and kinetic mixing strength can be probed down to $(1.4 - 10) \times 10^{-4}$ for dark photon mass between 15 GeV to 2 TeV. We also investigate the sensitivity of a future muon collider suggested by the muon accelerator program (MAP) to the dark photon model at different center-of-mass energies. It is shown that a future muon collider is able to reach a sensitivity to kinetic mixing at the order of 10^{-4}.

DOI: 10.1103/PhysRevD.106.015028

I. INTRODUCTION

Hidden sector states show up in several extensions of the Standard Model (SM) [1–8] to explain thermal relic WIMP dark matter [9–12], electroweak baryogenesis [13], hierarchy and naturalness [14–16]. The hunt for dark sector physics and hidden sector degrees of freedom are one of the major components of the physics program at the High Luminosity LHC (HL-LHC) and future colliders, such as future circular collider (FCC) [17–19], lepton colliders [20–22], and future muon collider [23–25].

In general, physics of dark sector could be characterized by the dark sector particle content and the mediators that connect the dark states to the SM fields. The interactions between the SM and dark sector content could be written either in terms of renormalizable or non-renormalizable operators [26]. The approach of non-renormalizable operators is suitable when the masses of dark sector mediators are larger than the energy scale of the process under consideration. In such a case, the mediators can be integrated out, and the interactions can be described in terms of contact non-renormalizable operators. On the contrary, if the mediators are light with respect to the energy scale of the process in the experiment, they can be produced on shell, and the interactions could be described in terms of renormalizable operators, which is the approach, we follow in the present work. So far, substantial study has been performed to search for dark photon (Z_D), which is a hypothetical massive vector boson mediating the interactions of dark matter particles [27–40]. Dark photon does not directly couple to SM fields; however, it can receive a small coupling to the electromagnetic current from the kinetic mixing between the Z_D and SM hypercharge. This coupling, which is tiny with respect to that of the SM photon by a factor labeled ϵ, would provide a possibility through which Z_D can be produced in the laboratory, and also it allows Z_D to decay into visible SM particles [26]. The kinetic mixing ϵ is an arbitrary parameter; however, special ranges of ϵ are interesting, which come from the loop level effects of heavier particles. Particularly, quantum effects of a heavy state that carries both SM hypercharge and $\mathrm{U}(1)_D$ charge typically generate $\epsilon \sim 10^{-4}$–10^{-2} [41–43]. Therefore, probing ϵ in the motivated region is one of the main goals of searches in dark sector physics. The value of kinetic mixing ϵ determines the dark photon lifetime. For small kinetic mixing values, Z_D has a long lifetime, so therefore it decays at a macroscopic distance from the point it is produced [3]. In this work, the concentration is on values of the kinetic mixing with m_{Z_D} above ~20 GeV that the dark photons decay promptly.

Clarification of the open questions in the SM and the observed consistency between the current LHC data and SM predictions has increased the desire to HL-LHC and has revived the interest of the community into a multi-TeV

Published by the American Physical Society under the terms of the Creative Commons Attribution 4.0 International license. Further distribution of this work must maintain attribution to the author(s) and the published article's title, journal citation, and DOI. Funded by SCOAP³.

muon collider program [23–25]. One of the marvelous advantages of utilizing muon beams is less radiation than electrons in a circular collider. While there are challenges such as the difficulties of achieving high intensity and low emittance muon beams, recent developments as well as potential alternative ways to achieve high intensity muon beams may lead to overcome the present limitations in the coming few years. Therefore, multi-TeV muon colliders could provide a new way to reach the energy frontier and to allow direct production of new heavy states.

In the first part of this paper, we derive constraints on dark photon interactions from partial wave unitarity, examining the allowed $VV \to VV$ scattering processes in the limit of large center-of-mass energies, where $V = W, Z$. The second part of the article is dedicated to collider searches for the dark sector. Dilepton production and dilepton production in association with a photon at the HL-LHC are revisited as processes to probe dark photon. Drell-Yan process at the HL-LHC has been already used in Refs. [3,44,45] in search for dark photon. In the present work, instead of repeating their analyses, a more detailed study using the expected differential rates including realistic detector effects and all sources of background processes is performed. As a complementary channel, a study is also carried out using dilepton production plus a photon at the HL-LHC. For this process, a test statistic is performed on the invariant mass of final state to derive sensitivity. Then, for the first time, the Drell-Yan process at a multi-TeV muon collider is used to probe the dark sector. Due to the high energy and precision, the future multi-TeV muon colliders offer a golden opportunity to probe dark photon parameter space.

The organization of this paper is as follows. Section II briefly describes the theoretical framework. Section III is dedicated to obtain the unitarity constraints using the $VV \to VV$ scatterings at high energies. In Sec. IV, we describe the analyses for determining the potential of HL-LHC to probe dark photons using the Drell-Yan and Drell-Yan in association with a photon in proton-proton collisions at $\sqrt{s} = 14$ TeV using 3000 fb^{-1} integrated luminosity of data. In Sec. IV, we also obtain prospects of a future multi-TeV muon collider at different center-of-mass energies and discuss the impact this has on our limit projections. Section V contains our conclusions.

II. THEORETICAL FRAMEWORK

Dark sectors commonly comprise one or more mediator states, which couple to the SM through a portal. The portal describing the interactions of dark sector with SM is dependent on the spin and parity of mediators. In general, the mediator can be a fermion, a vector, a scalar, or a pseudoscalar. In this work, we restrict ourselves to a simple dark photon model based on the extension of the SM gauge group to $\mathrm{SU}(3)_C \times \mathrm{SU}(2)_L \times \mathrm{SU}(2)_Y \times \mathrm{U}(1)_D$, where there is a kinetic mixing between a dark Abelian gauge symmetry, $\mathrm{U}(1)_D$ and the SM $\mathrm{U}(1)_Y$. In such an approach, a dark Higgs field S with nonzero vacuum expectation value is used to break the new dark $\mathrm{U}(1)_D$ symmetry. The related gauge terms in the Lagrangian are

$$L \supset -\frac{1}{4}\hat{Z}_{D\mu\nu}\hat{Z}_D^{\mu\nu} - \frac{1}{4}\hat{B}_{\mu\nu}\hat{B}^{\mu\nu} + \frac{1}{2}\frac{\epsilon}{\cos\theta_W}\hat{Z}_D^{\mu\nu}\hat{B}_{\mu\nu}, \quad (1)$$

where the hatted fields are gauge eigenstates, $\hat{Z}_D^{\mu\nu} = \partial^\mu \hat{Z}_D^\nu - \partial^\nu \hat{Z}_D^\mu$ and $\hat{B}^{\mu\nu} = \partial^\mu \hat{B}^\nu - \partial^\nu \hat{B}^\mu$, denote the dark photon and SM hypercharge field strengths, respectively. $\cos\theta_W$ is the cosine of Weinberg angle, and ϵ is the kinetic mixing parameter. The mass eigenstates of gauge boson are obtained by performing a rotation on the three neutral components of the gauge fields $\hat{B}, \hat{Z}_D$, and W_3 where a new mixing angle α appears:

$$\tan\alpha = \frac{1 - \delta^2 - \eta^2\sin^2\theta_W - \mathrm{Sign}(1-\delta^2)\sqrt{4\eta^2\sin^2\theta_W + (1 - \eta^2\sin^2\theta_W - \delta^2)^2}}{2\eta\sin\theta_W}, \quad (2)$$

where

$$\eta = \frac{\epsilon}{\cos\theta_W\sqrt{1 - \frac{\epsilon^2}{\cos^2\theta_W}}}, \quad (3)$$

and δ relates the dark vector mass to SM Z-boson mass before mixing; i.e., $m^2_{Z_D,0} \equiv \delta^2 \times m^2_{Z,0}$, where $m_{Z_D,0}$ and $m_{Z,0}$ are the dark photon and SM Z-boson masses before mixing. θ_W is the Weinberg angle.

More details of the formulating of the model can be found in Refs. [3,26]. The interaction between Z, Z_D-boson and the SM fermions has a form of $g_{Z_{(D)}f\bar{f}}Z_{\mu(D)}\bar{f}\gamma^\mu f$, where

$$\begin{aligned} g_{Zf\bar{f}} &= \frac{g}{\cos\theta_W}(\cos\alpha(T^3\cos^2\theta_W - Y\sin^2\theta_W) \\ &\quad + \eta\sin\alpha\sin\theta_W Y), \\ g_{Z_Df\bar{f}} &= \frac{g}{\cos\theta_W}(-\sin\alpha(T^3\cos^2\theta_W - Y\sin^2\theta_W) \\ &\quad + \eta\cos\alpha\sin\theta_W Y), \end{aligned} \quad (4)$$

where f is the left- or right-handed fermion, and Y and T^3 are the third component of hypercharge and weak isospin of the fermion f, respectively. The potential describing the SM Higgs and the dark Higgs sector has the following form:

$$V(H,S) = -\mu^2|H|^2 + \lambda|H|^4 - \mu_S^2|S|^2 + \lambda_S|S|^4 + \kappa_{HS}|H|^2|S|^2, \quad (5)$$

where S is the singlet dark Higgs field, and the SM Higgs doublet is denoted by H. The dark Higgs S and SM Higgs fields are linked through a renormalizable parameter κ_{HS}. Requiring the stability of the potential at large field values points to the requirement $\lambda, \lambda_S > 0$ and $\kappa_{HS} \geq -2\sqrt{\lambda\lambda_S}$ [46]. The constraint obtained from the requirement of perturbative unitarity leads to $\kappa_{HS} \leq 8\pi$ [47]. Indirect and direct constraints on dark Higgs mass and the corresponding mixing have been obtained in Ref. [48]. After spontaneous symmetry breaking, the mixing between the dark Higgs and SM Higgs is defined by θ_h angle, which is related to κ_{HS} in Eq. (5) via the following relation:

$$\tan\theta_h = \frac{\lambda v^2 - \lambda_S v_S^2 - \mathrm{Sign}(\lambda v^2 - \lambda_S v_S^2)\sqrt{\lambda^2 v^4 + \lambda_S^2 v_S^4 + v^2 v_S^2(\kappa_{HS}^2 - 2\lambda\lambda_S)}}{\kappa_{HS} v v_S}, \quad (6)$$

where v and v_S are the vacuum expectation values of the SM Higgs and the singlet scalar, which generates dark Higgs mass. For small mixing angles [3],

$$\tan\theta_h \approx \frac{\kappa_{HS}}{2} \times \frac{v v_S}{\lambda_S v_S^2 - \lambda v^2}. \quad (7)$$

There are several extensive experimental and phenomenological studies on searching for dark photon. The LHCb experiment searches are done for both promptlike and long-lived dark photons using the events produced in proton-proton collisions at a center-of-mass energy of 13 TeV [30]. The search is based on the dimuon decays using data corresponding to an integrated luminosity of 5.5 fb^{-1}. No evidence for dark photon has been found, and stringent exclusion limits at 90% confidence level are determined on the kinetic mixing strength on the mass region $0.214 < m_{Z_D} < 0.740$ GeV and $10.6 < m_{Z_D} < 30$ GeV. Another search has been performed by the CMS collaboration for a narrow resonance decaying to a dimuon pair using proton-proton collision data corresponding to an integrated luminosity of 137 fb^{-1} [27]. No deviation from the SM prediction has been observed in the explored mass ranges. Constraints on the kinetic mixing have been derived over the mass region of dark photon in the range of 30–75 GeV and 110–200 GeV.

In Ref. [3], it has been shown that the direct Drell-Yan production provides high sensitivity to dark photon and can probe $\epsilon \geq 9 \times 10^{-4}$ at the HL-LHC and $\epsilon \geq 4 \times 10^{-4}$ at the FCC-hh with $\sqrt{s} = 100$ TeV. Indirect constraints from the global fits to electroweak precision observables from the measurements at LEP, Tevatron, and the LHC have been also obtained in Ref. [3] which excludes $\epsilon \gtrsim 3 \times 10^{-2}$ for $5 \lesssim m_{Z_D} \lesssim 100$ GeV. There are bounds on dark photon parameters from beam-dump experiments [49–51], fixed-target experiments [52], and rare meson decays [53]. In Ref. [54], an estimate for a dark photon search at the LHeC and FCC-he through the dark photon displaced decays into two charged particles and in a mass range of 10 to 700 MeV has been studied. The LHeC (FCC-he) can exclude dark photons in the considered mass range with ϵ larger than $2 \times 10^{-5}(10^{-5})$.

In the next section, limits on dark photon interactions from partial wave unitarity are derived from the $VV \to VV$ scattering processes.

III. UNITARITY CONSTRAINTS

Violation of the partial wave unitarity indicates that new fundamental degrees of freedom or new composite states must be present around or below the scale of unitarity violation to preserve a physical behavior of scattering amplitudes. Unitarity requirement imposes consistency conditions on the theory parameters to be valid up to a given energy scale. On the other hand, for given values of the dark photon parameters, unitarity imposes an upper bound on the energy scale at which the theory is valid. We obtain constraints on the kinetic mixing from the partial wave unitarity, examining $VV \to VV$ scattering processes in the limit of large center-of-mass energy. A natural version of the unitarity requirement is [55]

$$|\mathrm{Re}(a_0)| \leq \frac{1}{2}, \quad (8)$$

where a_0 is corresponding to the $J = 0$ partial wave:

$$a_0 = \frac{1}{32\pi}\int_{-1}^{+1} \mathcal{M}(\cos\theta) d\cos\theta. \quad (9)$$

There are several s- and t-channel diagrams containing the exchange of a dark photon Z_D, Z, γ, and Higgs boson combined with the four-point interaction for the elastic scattering of $W^+W^- \to W^+W^-$. Representative Feynman diagrams for $W^+W^- \to W^+W^-$ scattering are depicted in Fig. 1. In addition to Z_D, there are contributions from dark Higgs boson to the $W^+W^- \to W^+W^-$ scattering. These contributions are expected to be small in the low mass region of dark Higgs boson as the coupling of dark Higgs with W^+W^- is proportional to $m_W^2 \sin\theta_h / v$ [48]. At low mass region $m_S \lesssim 10$ GeV, any value of θ_h above $\sim 10^{-4}$

has been excluded from LHCb [56,57], BNL-E949 [58], CHARM [59], LSND [60], and MicroBooNE [61] experiments. A summary of the reach from the present and proposed experiments for a dark Higgs boson are depicted in Ref. [62]. As a result, the contribution of light dark Higgs in the partial wave amplitude a_0 is suppressed by a factor of $(m_W^2 \sin\theta_h/v)^2 \lesssim \mathcal{O}(10^{-6})$.

Total amplitude for all contributing diagrams in the high energy limit has the following form:

$$\mathcal{M}_{\text{total}} = -\frac{g^2 m_H^2}{4m_W^2}\left(\frac{s}{s-m_H^2}+\frac{\frac{s}{2}(1-\cos\theta)}{\frac{s}{2}(1-\cos\theta)+m_H^2}\right)-\frac{\sin^2\theta_h s}{2v^2}(1+\cos\theta)-\frac{\sin^2\theta_h m_S^2}{v^2}\left(\frac{s}{s-m_S^2}+\frac{\frac{s}{2}(1-\cos\theta)}{\frac{s}{2}(1-\cos\theta)+m_S^2}\right)$$
$$-\frac{g^2 s}{4m_W^4}\sin^2\alpha\cos^2\theta_W\left(\frac{3s}{2}\cos\theta+\frac{3m_{Z_D}^2}{2}(1+\cos\theta)+\frac{s}{4}(\cos^2\theta-3)-8m_W^2\cos\theta\right), \tag{10}$$

where s is the center-of-mass energy, θ is the scattering angle, m_H is SM Higgs boson mass, m_S is dark Higgs mass, and m_W is W boson mass. After integration over $\cos\theta$ from -1 to 1, we find:

$$\int_{-1}^{+1}\mathcal{M}_{\text{total}}d\cos\theta = -\frac{g^2 m_H^2}{4m_W^2}\left(\frac{2s}{s-m_H^2}+2-\frac{2m_H^2}{s}\ln\left[1+\frac{s}{m_H^2}\right]\right)-\frac{\sin^2\theta_h s}{v^2}-\frac{\sin^2\theta_h m_S^2}{v^2}\left(\frac{2s}{s-m_S^2}+2-\frac{2m_S^2}{s}\ln\left[1+\frac{s}{m_S^2}\right]\right)$$
$$-\frac{g^2 s}{4m_W^4}\sin^2\alpha\cos^2\theta_W\left(3m_{Z_D}^2-\frac{4}{3}s\right). \tag{11}$$

As it can be seen, the scattering amplitude grows as the center-of-mass energy increases. It is notable that the term proportional to s arises from the diagram where dark photon Z_D is exchanged. The contribution of dark photon leads to unitarity violation at high energies. The partial wave amplitude a_0 in the high energy limit where $m_S^2, m_H^2 \ll s$ becomes

$$a_0 = -\frac{m_H^2}{8\pi v^2}-\frac{s}{32\pi v^2 m_W^2}\sin^2\alpha\cos^2\theta_W\left(3m_{Z_D}^2-\frac{4}{3}s\right)$$
$$-\frac{\sin^2\theta_h m_S^2}{8\pi v^2}-\frac{\sin^2\theta_h s}{32\pi v^2}. \tag{12}$$

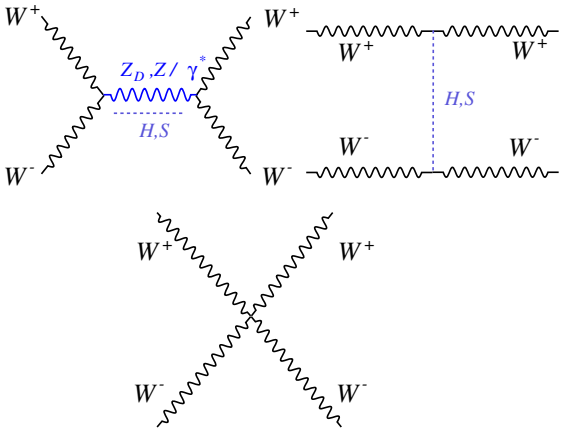

FIG. 1. Representative Feynman diagrams contributing to $W^+W^- \to W^+W^-$ scattering. In this figure, H is the SM Higgs boson, and Z_D is dark photon.

Applying the partial wave unitarity condition in Eq. (8), one finds upper limits on ϵ for different masses of the dark photon. In the left panel of Fig. 2, the upper limit on kinetic mixing strength ϵ versus the center-of-mass energy for four choices of the dark photon mass and for two cases of ($\theta_h = 0.001, m_S = 1$ GeV) (top) and ($\theta_h = 0.1, m_S = 200$ GeV) (bottom) is presented. As expected, the constraint on ϵ gets tighter as $\sqrt{s}$ grows. Among different masses, for m_{Z_D} close to the Z boson mass, the best sensitivity is achieved; however, with increasing m_{Z_D}, weaker bounds on ϵ are obtained. In the right plot of Fig. 2, an upper constraint on ϵ in terms of dark photon mass for three assumptions of center-of-mass energies of $\sqrt{s} = 0.1E_{\text{cm}}, 0.5E_{\text{cm}}$ and E_{cm} is presented. In deriving the limits, the value of E_{cm} is set to 13 TeV. The higher $\sqrt{s}$ the stronger limit on ϵ. We find that for $m_{Z_D} \lesssim 50$ GeV, with the center-of-mass energy of $\sqrt{s} = 13$ TeV, any value of ϵ above 10^{-3} is excluded by the unitarity conditions. From a comparison of top and bottom plots in Fig. 2, no significant dependence on the dark Higgs and the mixing angle is observed, which is expected in particular at low mass values. At the end of this section, it is worth mentioning that the bounds derived from $ZZ \to ZZ$ are found to be 2 orders of magnitude looser than those obtained from $WW \to WW$, and at lowest order, $Z_DZ_D \to Z_DZ_D$ process provides no constraints on ϵ since the amplitude has no dependence on ϵ.

IV. COLLIDER SEARCHES

The planned HL-LHC at 14 TeV with an integrated luminosity of 3000 fb^{-1}, future hadron and electron-positron colliders, and multi-TeV muon colliders provide excellent

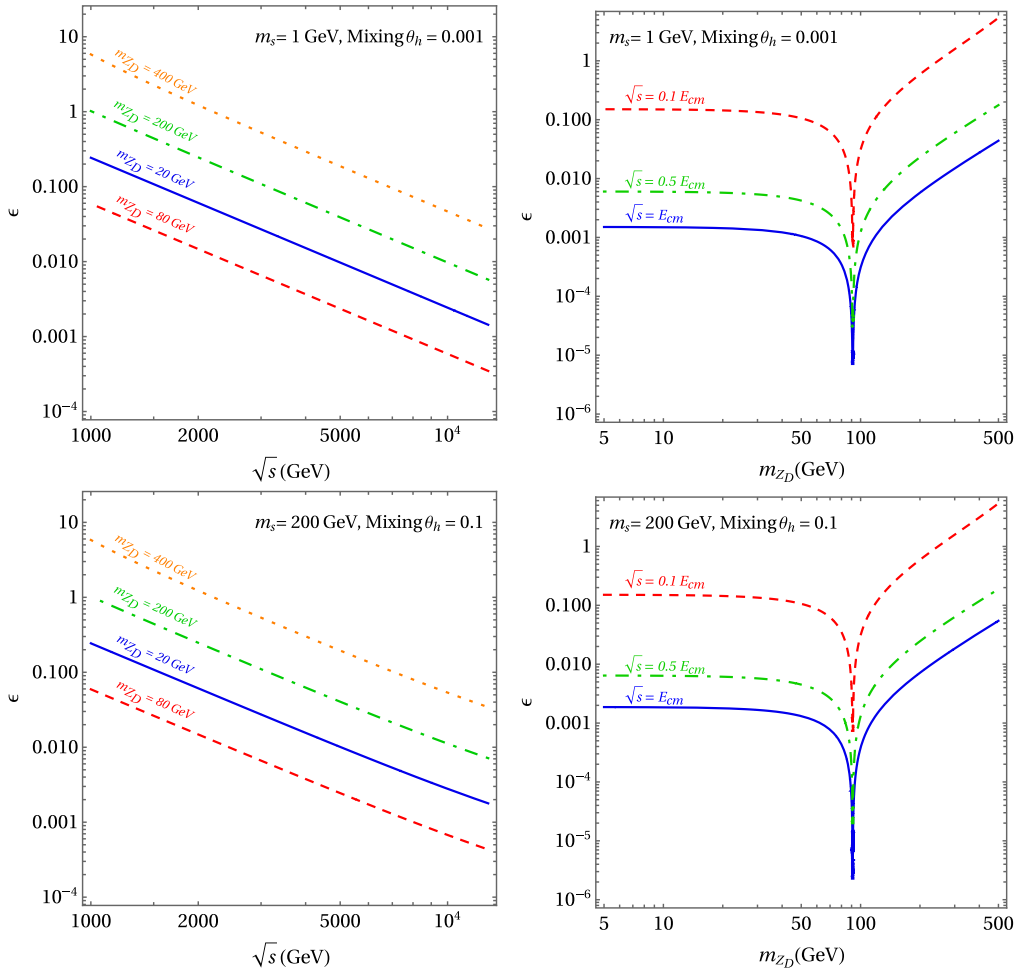

FIG. 2. Left: the upper limit on ϵ is shown versus $\sqrt{s}$ for $m_{Z_D} = 20$, 80, 200, and 400 GeV assuming $(\theta_h = 0.001, m_S = 1\ \text{GeV})$ (top) and $(\theta_h = 0.1, m_S = 200\ \text{GeV})$ (bottom). Right: upper bound on ϵ in terms of m_{Z_D} for three choices of center-of-mass energies of $\sqrt{s} = 0.1E_{\text{cm}}, 0.5E_{\text{cm}}$ and E_{cm}, where E_{cm} is assumed to be 13 TeV. The bounds are shown for $(\theta_h = 0.001, m_S = 1\ \text{GeV})$ (top) and $(\theta_h = 0.1, m_S = 200\ \text{GeV})$ (bottom).

opportunities to explore dark photon. In this section, we revisit the potential of the HL-LHC to probe the dark photon using Drell-Yan and Drell-Yan associated with a photon. We also present the prospect of a multi-TeV future muon collider to probe dark photon through Drell-Yan process. In all of the analyses presented in this section, ϵ and m_{Z_D} are probed, and it is assumed that the dark Higgs is heavy and the mixing κ_{HS} is set to a very small value ($\kappa_{HS} \sim 10^{-10}$).

A. Dilepton production through dark photon at the LHC

One of the processes that provides an excellent sensitivity to dark photon is the Drell-Yan production process, $pp \to Z_D$. Among the decay modes of Z_D, the hadronic decay mode of Z_D is the major decay channel; however, due to large contribution of multijet background, it is hard to achieve good sensitivity. On the other hand, the leptonic decay mode of Z_D has smaller background, and lepton reconstruction and identification efficiency and energy resolution are much better than those for jets. In Ref. [3,44,45], the HL-LHC potential to search for Z_D have been estimated using the Drell-Yan process in the presence of dark photon. In this section, it is shown that the $|\Delta\eta| = |\eta_{\ell^+} - \eta_{\ell^-}|$ distribution is a sensitive variable to search for dark photon in $pp \to Z_D \to \ell^+ + \ell^-$. We consider the main sources of background processes and take into account a CMS-like detector effects to probe the parameter space of dark photon. The dominant SM backgrounds to the assumed signal process are SM Drell-Yan $pp \to Z/\gamma^* \to \ell^+ + \ell^-$; production of two massive gauge bosons WW, WZ, ZZ where the W and Z bosons can decay leptonically and/or hadronically; Drell-Yan production of $\tau^+\tau^-$ with their subsequent decays to electron and muon pairs; $t\bar{t}$ in particular in the dileptonic decay mode; single top in tW-channel; and misidentified contribution where jets are misidentified as leptons.

Consider the lepton pair production through an intermediate Z_D, Z boson or a photon in proton-proton

collisions at the LHC. The cross section and differential cross sections can be factorized as follows:

$$\frac{d\sigma(pp\to\ell^+\ell^-)}{dm_{\ell\ell}}=\sum_{q,\bar{q}}\int dx_1dx_2f_q(x_1,Q)f_{\bar{q}}(x_2,Q)\times\frac{d\hat{\sigma}(q\bar{q}\to\ell^+\ell^-)}{dm_{\ell\ell}},\tag{13}$$

where $m_{\ell\ell}$ is the invariant mass of dilepton, $x_{1,2}$ are the momentum fractions of the quark q and anti-quark $\bar{q}$ partons in the protons, and $f_{q,\bar{q}}(x_i,Q)$ are the proton parton distribution functions, which are dependent on a factorization scale Q. The invariant mass is related to the center-of-mass energy via $m_{\ell\ell}=\sqrt{\hat{s}}=\sqrt{x_1x_2S}$, where $\sqrt{\hat{s}}$ and $\sqrt{S}$ are the partonic center-of-mass energy and center-of-mass energy, respectively. The cross section of dilepton production consists of terms arising from exchange of γ, Z, Z_D, as well as the interference terms [63]:

$$\frac{d\sigma(pp\to\ell^+\ell^-)}{dm_{\ell\ell}}=\frac{d\sigma_{\gamma\gamma}}{dm_{\ell\ell}}+\frac{d\sigma_{ZZ}}{dm_{\ell\ell}}+\frac{d\sigma_{Z_DZ_D}}{dm_{\ell\ell}}+2\frac{d\sigma_{\gamma Z}}{dm_{\ell\ell}}+2\frac{d\sigma_{\gamma Z_D}}{dm_{\ell\ell}}+2\frac{d\sigma_{ZZ_D}}{dm_{\ell\ell}}.\tag{14}$$

The differential cross section of pure signal reads

$$\frac{d\sigma_{Z_DZ_D}}{dm_{\ell\ell}}=\sum_{q,\bar{q}}d\eta_{\ell^+}d\eta_{\ell^-}x_1f_q(x_1)x_2f_{\bar{q}}(x_2)\frac{2}{\sqrt{\hat{s}}}\frac{d\hat{\sigma}_{Z_DZ_D}}{d\Delta\eta},\tag{15}$$

where

$$\frac{d\hat{\sigma}_{Z_DZ_D}}{d\Delta\eta}=\frac{1}{32\pi N_c\cosh^2\frac{\Delta\eta}{2}}\frac{\hat{s}}{(\hat{s}-m_{Z_D}^2)^2+m_{Z_D}^2\Gamma_{Z_D}^2}\times\sum_{i=0}^{2}c_i^q\left(-\frac{e^{-\frac{\Delta\eta}{2}}}{2\cosh\frac{\Delta\eta}{2}}\right)^i,\tag{16}$$

where $N_C=3$, Γ_{Z_D} is the total width of dark photon. The partonic differential cross section for the interference terms has the following form:

$$\frac{d\hat{\sigma}_{ij}}{d\Delta\eta}=\frac{\hat{s}}{32\pi N_c}\frac{(\hat{s}-m_i^2)(\hat{s}-m_j^2)+m_im_j\Gamma_i\Gamma_j}{[(\hat{s}-m_i^2)^2+m_i^2\Gamma_i^2][(\hat{s}-m_j^2)^2+m_j^2\Gamma_j^2]}\times c_{2,ij}^q\frac{1}{\cosh^2\frac{\Delta\eta}{2}}\left(-\frac{e^{-\frac{\Delta\eta}{2}}}{2\cosh\frac{\Delta\eta}{2}}\right)^2,\tag{17}$$

where $i,j=\gamma,Z,Z_D$ and the $c_{0,1,2}^q$ coefficients are defined as

$$\begin{aligned}
c_0^q&=[(g_q^V)^2+(g_q^A)^2].[(g_\ell^V)^2+(g_\ell^A)^2]-4g_q^Vg_q^Ag_\ell^Vg_\ell^A,\\
c_1^q&=2c_0^q,\\
c_2^q&=[(g_q^V)^2+(g_q^A)^2].[(g_\ell^V)^2+(g_\ell^A)^2],\\
c_{2,ij}^q&=2[g_{q,i}^Vg_{q,j}^V+g_{q,j}^Ag_{q,j}^A].[g_{\ell,i}^Vg_{\ell,j}^V+g_{\ell,j}^Ag_{\ell,j}^A],
\end{aligned}\tag{18}$$

The vector and axial couplings $g_i^{V,A}$ for leptons and quarks to γ, Z, and Z_D are

$$\begin{aligned}
\gamma&:g_f^V=eQ_f,\quad g_f^A=0,\\
Z&:g_f^V=\frac{e}{\sin\theta_W\cos\theta_W}\left(\cos\alpha\left(\frac{T_3}{2}-Q_f\sin^2\theta_W\right)-\eta\sin\alpha\sin\theta_W\left(\frac{T_3}{2}-Q_f\right)\right),\\
Z&:g_f^A=\frac{e}{\sin\theta_W\cos\theta_W}(\cos\alpha-\eta\sin\alpha\sin\theta_W)\frac{T_3}{2},\\
Z_D&:g_f^V=\frac{e}{\sin\theta_W\cos\theta_W}\left(-\sin\alpha\left(\frac{T_3}{2}-Q_f\sin^2\theta_W\right)-\eta\cos\alpha\sin\theta_W\left(\frac{T_3}{2}-Q_f\right)\right),\\
Z_D&:g_f^A=\frac{e}{\sin\theta_W\cos\theta_W}(-\sin\alpha-\eta\cos\alpha\sin\theta_W)\frac{T_3}{2},
\end{aligned}\tag{19}$$

where Q_f is fermion electric charge. Because the main irreducible background; i.e., Drell-Yan has exactly the same initial and final states as signal, and there is interference between signal and background at tree level appeared in Eq. (14) by $\sigma_{\gamma Z_D}$ and σ_{ZZ_D}. In Fig. 3, the normalized differential partonic cross section for signal + background and for Drell-Yan only is depicted. The signal curves belong to two choices of $m_{Z_D}=50$ and 1200 GeV with $\epsilon=0.05$. As one can see, at large $\Delta\eta$ values, the

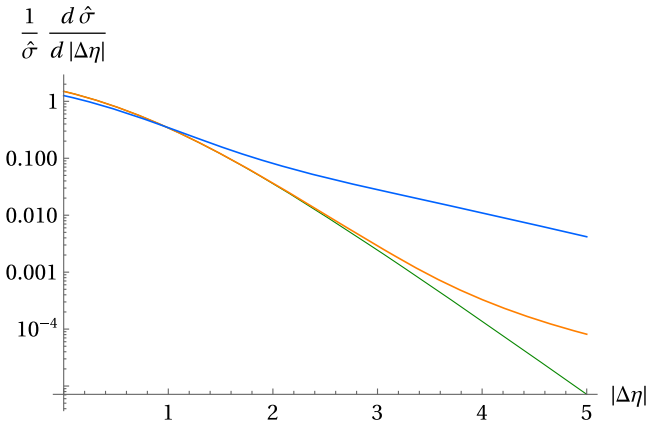

FIG. 3. The differential partonic cross section of $|\Delta\eta|=|\eta_{\ell^+}-\eta_{\ell^-}|$ for the SM, $m_{Z_D}=50$ and 1200 GeV assuming $\epsilon=0.05$. The SM expectation is depicted by the green curve, and the orange and blue curves present the SM + Z_D with $m_{Z_D}=50$ and 1200 GeV, respectively.

dilepton production rate gets separated from the SM Drell-Yan process and goes up visibly above the SM. This discrepancy is expected to be more important at large $\hat{s}$, which is corresponding to large m_{Z_D}. Therefore, more sensitivity to heavy dark photons is expected. In the following, this difference in shape is used to probe the dark photon parameter space.

The dark photon signal events are simulated with the MadGraph5-aMC@NLO Monte Carlo generator [64–66], and an already available Universal FeynRules Output (UFO) model [67].[1] The parton level events are passed through PYTHIA8 [68] to perform parton shower, hadronization and decay of unstable particles. As mentioned, the effects of detector are simulated with DELPHES3.3.2 package [69]. The simulated samples for background processes are also generated in a similar fashion. The selection of events is designed to identify opposite-sign charged lepton events compatible with the dilepton events arising from dark photon while suppressing the contribution of background processes. The analysis concentrates on events with prompt Z_D decays and not on displaced dark photon. In order to trigger the events, one can either rely on the single lepton or double lepton triggers. The charged lepton transverse momentum requirements are applied to satisfy the double lepton triggers. The leading lepton is required to have $p_{\mathrm{T}} > 25$ GeV, and the second lepton must have $p_{\mathrm{T}} > 20$ GeV. Pseudorapidity ranges are chosen to cover regions of good reconstruction quality. For electrons and muons, it is required that $|\eta| < 2.4$. The leptons are required to satisfy isolation criteria. The relative isolation for a charged lepton defined as

$$\mathrm{RelIso} = \frac{\sum_k^{\Delta R(\ell,k)<0.3} p_{\mathrm{T}}(k)}{p_{\mathrm{T}}(\ell)}, \tag{20}$$

where in the numerator, the sum is over the transverse momenta of particles residing inside a cone with a radius of $R = 0.3$, except the charged lepton. For both electrons and muons, it is required RelIso < 0.15. In addition, $\Delta R(\ell^+, \ell^-)$ is required to be larger than 0.3. To reduce the contribution of low-mass resonances and charged leptons from hadrons decays, the invariant mass of dilepton is required to be larger than 10 GeV. Furthermore, the transverse momentum of the lepton pair must satisfy $p_{\mathrm{T}}^{\ell\ell} > 30$ GeV to reduce background contributions from non-prompt leptons. In order to reduce background contributions from VZ ($V = W, Z$) production, events with a third, loosely identified charged lepton with $p_{\mathrm{T}} > 10$ GeV are discarded. For further background suppression, the magnitude of missing transverse momentum is required to be less than 20 GeV, and events containing any b jet with $p_T > 30$ GeV and $|\eta| < 2.4$ are discarded. This helps reduce the contributions from $t\bar{t}$ and single top tW channel. The normalized distribution of $|\eta_{\ell^+} - \eta_{\ell^-}|$ for dark photon with $\epsilon = 0.01, m_{Z_D} = 200$ GeV and for the main background processes after the above cuts are depicted in Fig. 4.

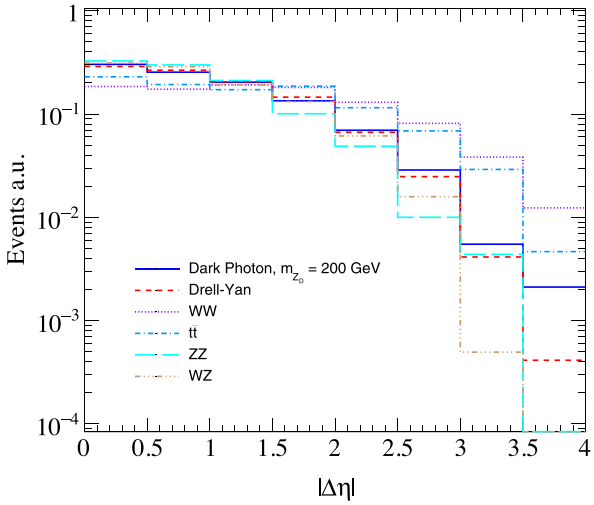

FIG. 4. The normalized distribution of $|\Delta\eta| = |\eta_{\ell^+} - \eta_{\ell^-}|$ for dark photon signal with $m_{Z_D} = 200$ GeV and for the main background processes of Drell-Yan, $t\bar{t}$, and diboson.

In order to obtain the projected sensitivity for the dark photon parameters, we define a χ^2 statistic over the $|\Delta\eta|$ distribution as follows:

$$\chi^2(\epsilon, m_{Z_D}) = \sum_{i\in\mathrm{bins}} \frac{(N^i_{\mathrm{SM+DP}}(\epsilon, m_{Z_D}) - N^i_{\mathrm{SM}})^2}{(\delta^i)^2}, \tag{21}$$

where $N^i_{\mathrm{SM+DP}}(\epsilon, m_{Z_D})$ denotes the number of events in the ith bin, after the selection cuts described above, and N^i_{SM} is the SM prediction. The uncertainties δ^i are both statistical and systematic uncertainties. Systematic uncertainties are taken from a CMS experiment analysis, where a differential cross section of Drell-Yan has been measured in both electron and muon channels [70]. The systematic uncertainties are considered differently in three mass regions of low mass (below 40 GeV), Z-boson peak region, and high mass region (above 200 GeV). In this work, on the electron and the muon channels, the systematic uncertainties related to the electron channel are applied. Since the uncertainties related to the electron channel are larger than the muon one, this makes the estimate of the sensitivities more conservative.

Confidence level intervals are then calculated using

$$1 - \mathrm{CL} = \int_{\chi^2}^{\infty} f_m(x)dx, \qquad \chi^2 = \chi^2(\epsilon, m_{Z_D}), \tag{22}$$

where $f_m(x)$ is the χ^2 distribution of m degrees of freedom evaluated considering the number of free parameters and the number of total bins. In order to increase the sensitivity,

[1] http://insti.physics.sunysb.edu/curtin/hahm_mg.html.

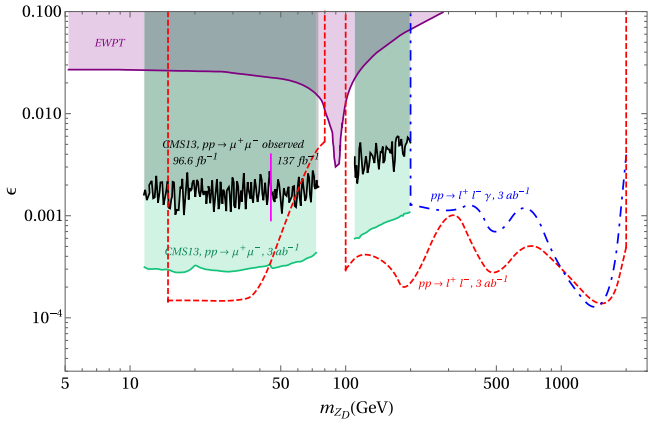

FIG. 5. Future projection constraints on $\epsilon - m_{Z_D}$ parameters at 95% CL from dark photon Drell-Yan production and dilepton production in association with a photon at the HL-LHC with 3 ab^{-1} are depicted as red dashed and blue dot-dashed lines, respectively. The black solid curve shows the observed upper limits on the kinetic mixing ϵ at 90% CL as a function of the dark photon mass using dimuon final state in proton-proton collision data collected by the CMS experiment at $\sqrt{s} = 13$ TeV with an integrated luminosity of 137 fb^{-1} [27]. The projection of the CMS experiment results from dimuon channel to an integrated luminosity of 3 ab^{-1} is also presented as the green solid curve. Bounds at 95% CL from the electroweak observables are presented as purple shaded region [3].

an additional cut is imposed on the dilepton invariant mass $m_{\ell\ell}$ so that the best sensitivity is achieved. For each m_{Z_D}, it is required the lepton pair in each event to satisfy: $\Delta_1 < |m_{\ell\ell} - m_{Z_D}| < \Delta_2$, where $\Delta_{1,2}$ are optimized separately for each value of m_{Z_D} to obtain the best limit on ϵ. The scan is performed using the χ^2 statistic calculated at an integrated luminosity of $L = 3000$ fb^{-1}, and the allowed region evaluated in the $\epsilon - m_{Z_D}$ plane at 95% confidence level is depicted in Fig. 5. For the Z_D mass range of 15 GeV to 2 TeV (except 60–100 GeV), any value of ϵ above $(1.4 - 10) \times 10^{-4}$ can be excluded using this analysis.

B. Dark photon production associated with a photon at the LHC

Within the SM, studying Z boson production in association with a photon at the LHC plays an important role as it provides crucial tests of the electroweak sector. The $Z + \gamma$ measurements are used to search for the effects of new physics beyond the SM such as direct couplings of Z bosons to photons. There are measurements for the inclusive and differential $Z + \gamma$ production cross sections using different datasets collected at center-of-mass energies and in $\ell^+\ell^-$, $\nu\nu$, and $b\bar{b}$ channels by the ATLAS and CMS collaborations [71–74]. Compared to the $b\bar{b} + \gamma$ and $\nu\nu + \gamma$ channels, the $\ell^+\ell^- + \gamma$ channel provides the possibility for cross section measurements with lower background contributions and less uncertainties from systematic sources. Therefore, in addition to dilepton production from dark photon, $\ell^+\ell^-\gamma$ channel with its clean final state and under-control systematic sources can be used to probe dark photon physics. In this section, the focus is on search for dark photon in $pp \to \ell^+\ell^-\gamma$ considering a realistic CMS-like detector effects and the main sources of background processes.

The dominant background to the $\ell^+\ell^-\gamma$ signal comes from the SM $\ell^+\ell^-\gamma$ events. Other background contributions arise from $t\bar{t}\gamma$ (with one or both top quarks decaying semileptonically), VV, $VV\gamma$ (where $V = W, Z$) (including W and Z bosons decays to final states involving τ-leptons). There are contributions to the background composition from events containing Higgs boson with $H \to Z + \gamma$ decays where $Z \to \ell^+\ell^-$, which is found to be negligible after the full selection described below.

Similar to the previous analysis described in Sec. IV A, the signal and background processes are generated using MadGraph5-aMC@NLO event generator, then PYTHIA8 to perform parton shower, hadronization, and decay of unstable particles, and the impact of a CMS-like detector is simulated with DELPHES3.3.2.

Signal events are selected by requiring the existence of a photon together with a same-flavor lepton (e or μ) pair. The contributions from background events coming from processes producing nonprompt leptons or photons are significantly suppressed by applying isolation requirements on the photon candidate and the two leptons. Similar trigger requirements and isolation criteria as described in the Drell-Yan analysis are imposed on the leptons. Photon candidate is required to have a pseudorapidity in the range $|\eta| < 2.5$ and to have a transverse momentum greater than 20 GeV and the relative isolation RelIso < 0.15 as defined in Eq. (20). Events containing additional photons with $p_T > 20$ GeV, $|\eta| < 2.5$ and RelIso < 0.2 are rejected. In addition to the above requirements, photon candidates are required to be well separated from all electrons and muons in the event by $\Delta R(\ell^\pm, \gamma) > 0.3$, and lepton candidates are required to be separated from each other in the event by $\Delta R(\ell^-, \ell^+) > 0.3$. The magnitude of missing transverse momentum vector is required to be less than 20 GeV, which helps reduce the background containing neutrino(s) in the final state. To further suppress the contribution from $t\bar{t} + \gamma$, $VV\gamma$, and single top plus a photon, events that have any jet with $p_T > 30$ GeV and $|\eta| < 2.4$ are rejected. For the sake of reducing the contribution of backgrounds from low-mass resonances, charged leptons from hadrons decays, misidentified photon, and Z boson decays, a lower cut is applied on the invariant mass of dilepton. The concentration in this analysis is on the dark photon mass region above 200 GeV where the misidentified background contribution is suppressed. The signal efficiency for $m_{Z_D} = 400$ GeV and $\epsilon = 0.01$ is 2.0%. The efficiencies of SM $\ell^+\ell^-\gamma$, $t\bar{t}\gamma$, $WW\gamma$, $ZZ\gamma$, $WZ\gamma$ are 1.97%, 0.006%, 0.51%, and 1.03%, 1.58%, respectively.

Furthermore, there are background events from Drell-Yan + jets process containing nonprompt photons, for example, arising from π^0 or η^0 decays. The probability for a jet misidentified as a photon varies with the misidentified photon transverse momentum and is of the order of $\sim 10^{-3}(10^{-5})$ for low (high) p_T jets [75]. Its contribution is estimated to be less than 3% of the total background contribution in the signal region. We neglect this background in the analysis; nevertheless, a dedicated and a detailed detector simulation has to be performed to estimate it.

In order to assess the sensitivity, having obtained the predicted signal, a profile likelihood ratio test statistic is constructed over an optimised range of $m_{\ell\ell\gamma}$. The constraints on the kinetic mixing versus the dark photon mass at 95% CL are presented in Fig. 5 as dot-dashed blue curve. An overall systematic uncertainty from Ref. [76] is considered in extracting the limits. The limit is obtained using an integrated luminosity of 3 ab^{-1}. As can be seen, in the high mass region $m_{Z_D} \geq 200$ GeV, kinetic mixing parameter ϵ can be excluded for any value above $\sim 10^{-4}$.

C. Projection of $Z_D \to \mu^+\mu^-$ measurement at HL-LHC

In Ref. [27], CMS collaboration has performed a search for a dark photon decaying to a pair of muons $Z_D \to \mu^+ + \mu^-$ using data recorded at a center-of-mass energy of 13 TeV. The search has been done in the mass ranges of 45–75 GeV and 110–200 GeV using an integrated luminosity of 137 fb^{-1}. It should be indicated that the search in the mass range of 11.5–45.0 GeV has been carried out with 96.6 fb^{-1} data collected using high rate dimuon triggers. The result of this search is shown in Fig. 5 as black solid curve. The limits obtained using high rate dimuon triggers for the mass range of 11.5–45.0 GeV is separated from those derived with the standard triggers by a vertical pink line. For the Z_D mass range of 11.5–75 GeV (110–200 GeV), any value of kinetic mixing parameter above $(1-2)\times 10^{-3}((2-5)\times 10^{-3})$ has been excluded by this analysis. An extrapolation of the expected results to an integrated luminosity of 3 ab^{-1} is performed, which are presented in Fig. 5 as green solid curve. As seen, increasing the integrated luminosity to HL-LHC benchmark would improve the constraints on kinetic mixing parameter ϵ by a factor of ∼6–7.

We note that stronger limits from the Drell-Yan Z_D production using a shape analysis on $\Delta\eta$ distribution (red dashed curve in Fig. 5) is achieved as compared to the extrapolation of CMS experiment results (green solid curve in Fig. 5). Different behavior of $\Delta\eta$ distribution with respect to the SM background in particular for heavy dark photons is the main reasons for this potential improvement. It is notable that performing the shape analysis on $\Delta\eta$ distribution with only dimuon channel loosens the constraints around 15%–25% depending on the dark photon mass. It is found that at large Z_D masses $m_{Z_D} \gtrsim 800$ GeV, the resulting limits from dark photon Drell-Yan are comparable with those derived from $\ell^+\ell^-\gamma$ signature. In the dark photon mass region 200 to 800 GeV, $\ell^+\ell^-\gamma$ limits are slightly weaker than those of Z_D production.

D. Prospects for a multi-TeV muon collider

Muon colliders are in particular noticed due to several potential benefits such as availability of the full energy of muons in collisions, clean environment compared to hadron colliders, and significant mass suppressed synchrotron radiation with respect to the electron-positron colliders. They are excellent options, which allow us to scan the Higgs boson resonance and to accurately measure its mass and width. In addition, muon colliders are ideal to probe new physics effects beyond the SM and to study narrow resonances both as machines for precision and for exploratory purposes. The aim of this section is to present the potential of a future muon collider in search for dark photon and its ability to scan the dark photon parameter space.

We perform the search through the singly produced Z_D in the s channel via Drell-Yan production, i.e., $\mu^+ + \mu^- \to \ell^+ + \ell^-$ with $\ell = e, \mu$. The sensitivity of dilepton measurements to dark photon can be obtained from dilepton mass spectrum measurement or other differential distributions. Both in electron and muon colliders, photon radiation is the effect that needs to be considered when a narrow resonance is created in the annihilation channel. Such an effect has been important in observation of J/ψ in electron-positron collisions and in Z-boson production [77–79]. Photon radiation in dark photon production at $\mu^+\mu^-$ collisions leads to the following modification factor in the lowest order cross section:

$$\left(\frac{\Gamma_{Z_D}}{m_{Z_D}}\right)^{\frac{4\alpha}{\pi}\log(\sqrt{s}/m_\mu)}, \tag{23}$$

where Γ is the width of dark photon, s is the center-of-mass energy of the collision, and m_μ is the muon mass. Such QED effects have been accurately calculated for the experiments at the large electron positron (LEP) collider up to two-loop corrections [80]. As for the studies in muon colliders, these corrections have been mentioned in studies related to Higgs boson line shape and design of machine. For example, the impact of this modification factor on Higgs boson production rate is expected to be of the order of 50% [81]. As seen in Eq. (23), this reduction factor depends on the center-of-mass energy so that the higher $\sqrt{s}$ the larger suppression rate. For large dark photon masses compared to Z boson $m_{Z_D} > m_Z$ and small values of the strengths of kinetic mixing $\epsilon \ll 1$, $\Gamma_{Z_D}/m_{Z_D} < \Gamma_Z/m_Z$, where $\Gamma_Z/m_Z = 0.02$. Therefore, in this region of parameter space ($m_{Z_D} > m_Z$ and $\epsilon \ll 1$), the suppression factor for Drell-Yan dark photon is greater than SM Drell-Yan,

and as a result, more photon radiations are expected for SM Drell-Yan. This effect shows up for instance in $|\vec{p}_T^{\ell\ell}|$ distribution as more photon radiations give rise to further imbalance in momentum of dilepton in the final state. In this section, based on the difference between the shape of SM Drell-Yan, which is the main irreducible background and the dark photon signal in $|\vec{p}_T^{\ell\ell}|$ distribution, the sensitivity to parameter space is derived.

According to the dilepton final state, there are different SM background processes. The SM $\ell^+\ell^-$ production, W^+W^- when both of the W bosons decay leptonically, ZZ when at least one of the Z bosons decays to a lepton pair, top quark pair in dilepton decay mode, and HZ when $Z \to \ell^+ + \ell^-$ are the main background processes. The background processes are generated using MadGraph5_aMC@NLO to produce hard events. Showering, hadronization, and decays of unstable particles are done with PYTHIA8. The impact of detector is simulated using DELPHES3.5.0 considering the DELPHES card for muon collider.[2] The analysis is performed for two center-of-mass energies 1.5 and 6 TeV.

The signal final state is composed of two oppositely charged same-flavour isolated leptons, electrons or muons, compatible with a Z_D boson decay. The cross section of signal is much lower than that of the major reducible and irreducible background processes, and therefore, an optimum selection is needed to obtain a sample of sufficient purity. To be consistent with the expected dark photon signal topology, the selection requires leptons (e, μ) with $p_T > 15$ GeV and pseudorapidities of leptons are required to be $|\eta| < 2.5$ for electrons and $|\eta| < 3.0$ for muons. Both electrons and muons have to be isolated by applying similar requirements on the RelIso variable to the LHC analysis as defined in Eq. (20), presented in Sec. IV A with a difference of the size of isolation cone which is taken to be 0.1. In addition, to ensure the charged leptons are well isolated, it is required that $\Delta R(\ell^+, \ell^-) > 0.3$. To reduce background processes containing neutrinos that appear as missing energy in the final state, the magnitude of missing transverse momentum is required to be less than 20 GeV, and the invariant mass of the dilepton system is required to be greater than $0.8 \times \sqrt{s}$. These suppress ZZ, top quark pair, and WW background remarkably. As indicated, the signal topology is characterized by a dilepton system; however, due to photon radiations from initial state and/or final state, the momentum of the dilepton system is not balanced, and a deviation in total momentum is expected. In Fig. 6, the magnitude of the total momentum of the dilepton system in the transverse plane is presented for signal with $m_{Z_D} = 200$ GeV and the strength of kinetic mixing of $\epsilon = 0.01$ and for the main irreducible SM Drell-Yan background, WW, and ZZ processes. At $\sqrt{s} = 1.5$ TeV, the efficiency of signal for $m_{Z_D} = 200$ GeV and $\epsilon = 0.01$ is found to be

[2]https://github.com/delphes/delphes/blob/master/cards/delphes_card_MuonColliderDet.tcl.

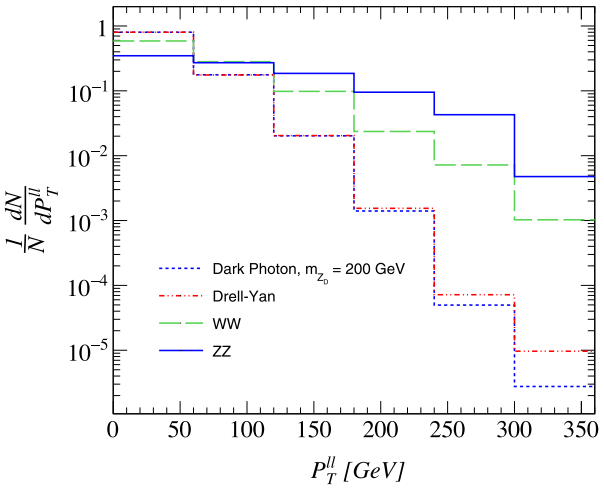

FIG. 6. Distributions of $|\vec{p}_T^{\ell\ell}|$ for dark photon signal with $m_{Z_D} = 200$ GeV and the strength of kinetic mixing of 0.01 at a center-of-mass energy of 1.5 TeV. The distributions for the main irreducible SM Drell-Yan background as well as WW and ZZ are depicted.

72.4%, and the efficiencies for background processes SM Drell-Yan, WW, ZZ, top quark pair, HZ are, respectively, 72%, 0.5%, 0.02%, $\lesssim 10^{-4}$%, and 0.0.

As expected, the distribution of $|\vec{p}_T^{\ell\ell}|$ for dark photon signal drops faster than the SM Drell-Yan. The distributions of WW and ZZ background processes have a remarkable tail at large values of $|\vec{p}_T^{\ell\ell}|$ because of the presence of neutrinos, which cause larger imbalance in the total momentum of the dilepton system. For the signal process, the differential distribution for $|\vec{p}_T^{\ell\ell}|$ can be written in the following form:

$$\frac{d\sigma(\epsilon, m_{Z_D})}{d|\vec{p}_T^{\ell\ell}|} = \frac{d\sigma_{\rm SM}}{d|\vec{p}_T^{\ell\ell}|} + \epsilon \frac{d\sigma_{\rm int.}(m_{Z_D})}{d|\vec{p}_T^{\ell\ell}|} + \epsilon^2 \frac{d\sigma_{Z_D}(m_{Z_D})}{d|\vec{p}_T^{\ell\ell}|}, \quad (24)$$

where $d\sigma_{\rm int.}(m_{Z_D})/d|\vec{p}_T^{\ell\ell}|$ and $d\sigma_{Z_D}(m_{Z_D})/d|\vec{p}_T^{\ell\ell}|$ are the interference term and the pure dark photon contribution, respectively. This allows us to scan the parameter space (ϵ, m_{Z_D}) using a χ^2 statistic on the $|\vec{p}_T^{\ell\ell}|$ distribution. The scan with the χ^2 statistic calculated at the center-of-mass energies of 1.5 TeV and 6 TeV is performed using the integrated luminosities of 0.2,1,2 ab^{-1}, and 4 ab^{-1}, respectively, and contours evaluated in the (ϵ, m_{Z_D}) plane at 95% confidence level are shown in Fig. 7. The average luminosities for a future muon collider as suggested by the muon accelerator program [24] at $\sqrt{s} = 1.5$ TeV and $\sqrt{s} = 6$ TeV are 1.25×10^{34} cm^{-2}s^{-1} and 12×10^{34} cm^{-2}s^{-1}, respectively. The integrated luminosity of 2 ab^{-1} at $\sqrt{s} = 1.5$ TeV is corresponding to five years of data taking, and the benchmark integrated luminosity of 4 ab^{-1} at $\sqrt{s} = 6$ TeV is taken from Ref. [25].

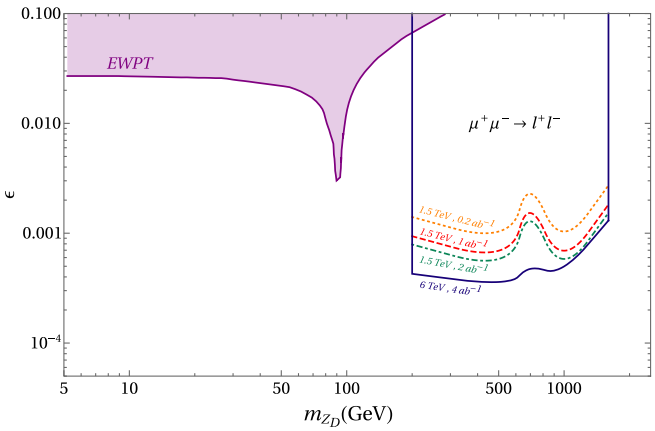

FIG. 7. Constraints on $\epsilon - m_{Z_D}$ plane at 95% CL from a muon collider at $\sqrt{s} = 1.5$ and 6 TeV with the integrated luminosities of (0.2,1,2) ab^{-1} and 4 ab^{-1}, respectively. Limits from the electroweak observables are given as purple shaded region at 95% CL [3].

As seen in Fig. 7, multi-TeV colliders at the center-of-mass energies of 1.5 TeV and 6 TeV offer sensitivity to $\epsilon \gtrsim 10^{-4}$ for dark photon with mass greater than 200 GeV to around 1 TeV. This is the same order of magnitude as exclusion limits achievable with searches based on direct Z_D production at the HL-LHC as presented in Fig. 5. As a final comment, we discuss some possible ideas to improve the search strategy and boost the sensitivity. Extending the final state to the hadronic decays of the dark photon in addition to the dilepton final state could be used as a good way to increase the signal statistics and improve the sensitivity. Exploiting multivariate techniques such as boosted decision trees (BDTs) or neural networks (NNs) by using effective discriminating variables help distinguish the dark photon signal from the dominant background sources, which would lead to obtain better results. Polarization of the muon beams can be used as a superior tool to probe dark photon and to handle background processes from signal as they have different chiral structures.

V. CONCLUSIONS

Dark sector states show up in many extensions of the Standard Model, which mainly serve as candidates for the dark matter in the universe. A dark sector can be proposed with an additional $U(1)_D$ dark gauge symmetry. It can interact with the SM through kinetic mixing with the hypercharge gauge boson where a kinetic mixing parameter ϵ deals with the coupling strength of the dark photon and SM particles. In this paper, firstly, we obtained bounds on dark photon parameters from partial wave unitarity, examining the allowed $WW \to WW$ scattering processes in the limit of large center-of-mass energy. The contribution of dark Higgs in the $WW \to WW$ is considered. The limits from unitarity examination depends on the center-of-mass energy of the WW scattering and found to be $\epsilon < 0.001$ for $m_{Z_D} \leq 50$ GeV and $\sqrt{s} = 13$ TeV. The results depend on the dark Higgs mass m_S and its mixing angle θ_h with the SM Higgs boson and are presented for small values of mixing angle θ_h. The bounds are not sensitive to m_S and θ_h because the dark Higgs coupling with WW is suppressed by $\sin\theta_h$.

The second part of the paper presented collider searches for dark photon. The presence of dark photon could lead to deviations from the SM predicted total and differential cross sections of processes like direct Z_D and Z_D production associated with a photon, which are used in the present work. These processes are golden channels for dark photon searches providing that the dark Higgs boson mixing with SM Higgs boson is small. Performing a fast detector simulation with DELPHES package and taking into account the main sources of background processes, scans were performed to constrain the dark photon parameter space using $pp \to Z_D \to \ell^+\ell^-$ and $pp \to \ell^+\ell^- + \gamma$. For Z_D production, it has been shown that the presence of dark photon modifies the $|\Delta\eta| = |\eta_{\ell^+} - \eta_{\ell^-}|$ distribution using analytical calculation. The $|\Delta\eta|$ distribution enables us to differentiate between signal and the main SM background processes. With performing a χ^2 fit on $|\Delta\eta|$ distribution, and limits on ϵ versus m_{Z_D} were derived at HL-LHC. Excluding Z boson mass window, for dark photon mass from 15–80 GeV and 200–2000 GeV, ϵ could be excluded down to $(1.4 - 10) \times 10^{-4}$. In $\ell^+\ell^- + \gamma$ search, a test statistic is performed over the $m_{\ell\ell\gamma}$ distribution to extract the limits. For $m_{Z_D} = 200$ GeV to 2000 GeV, constraints between 0.0002–0.001 obtained on ϵ at HL-LHC. The $\ell^+\ell^- + \gamma$ channel is a complementary channel to Z_D production at the LHC in particular for large mass of dark photon where less background contribution contribute in the spectrum.

Finally, we showed that multi-TeV muon colliders with the clean environment have excellent sensitivity to dark photons. Using $\mu^+ + \mu^- \to \ell^+ + \ell^-$ at $\sqrt{s} = 1.5$ and 6 TeV, considering detector effects and major sources of background, we showed that for m_{Z_D} above 200 GeV to around 1000 GeV, ϵ can be probed down to almost $(3 - 5) \times 10^{-4}$. Multi-TeV muon collider approaches the same sensitivity to dark photon as Drell-Yan process at the HL-LHC. Our conclusions for the dark photon sensitivity were based on a preliminary detector performance implemented in DELPHES, which may differ from the ultimate detector performance of possible muon colliders.

ACKNOWLEDGMENTS

The authors are grateful to Gh. Haghighat for reading the manuscript and useful comments.

[1] N. Arkani-Hamed, D. P. Finkbeiner, T. R. Slatyer, and N. Weiner, Phys. Rev. D **79**, 015014 (2009).
[2] P. Fayet, Phys. Rev. D **70**, 023514 (2004).
[3] D. Curtin, R. Essig, S. Gori, and J. Shelton, J. High Energy Phys. 02 (2015) 157.
[4] D. Curtin, R. Essig, S. Gori, P. Jaiswal, A. Katz, T. Liu, Z. Liu, D. McKeen, J. Shelton, and M. Strassler *et al.*, Phys. Rev. D **90**, 075004 (2014).
[5] S. Gopalakrishna, S. Jung, and J. D. Wells, Phys. Rev. D **78**, 055002 (2008).
[6] H. Davoudiasl, H. S. Lee, I. Lewis, and W. J. Marciano, Phys. Rev. D **88**, 015022 (2013).
[7] H. Davoudiasl, H. S. Lee, and W. J. Marciano, Phys. Rev. D **85**, 115019 (2012).
[8] J. D. Wells, arXiv:0803.1243.
[9] M. Pospelov, A. Ritz, and M. B. Voloshin, Phys. Lett. B **662**, 53 (2008).
[10] D. Feldman, B. Kors, and P. Nath, Phys. Rev. D **75**, 023503 (2007).
[11] J. L. Feng, Annu. Rev. Astron. Astrophys. **48**, 495 (2010).
[12] T. A. Porter, R. P. Johnson, and P. W. Graham, Annu. Rev. Astron. Astrophys. **49**, 155 (2011).
[13] D. E. Morrissey and M. J. Ramsey-Musolf, New J. Phys. **14**, 125003 (2012).
[14] N. Craig, S. Knapen, and P. Longhi, Phys. Rev. Lett. **114**, 061803 (2015).
[15] N. Craig and K. Howe, J. High Energy Phys. 03 (2014) 140.
[16] Z. Chacko, H. S. Goh, and R. Harnik, Phys. Rev. Lett. **96**, 231802 (2006).
[17] A. Abada *et al.* (FCC Collaboration), Eur. Phys. J. Special Topics **228**, 261 (2019).
[18] A. Abada *et al.* (FCC Collaboration), Eur. Phys. J. Special Topics **228**, 755 (2019).
[19] A. Abada *et al.* (FCC Collaboration), Eur. Phys. J. C **79**, 474 (2019).
[20] M. Aicheler, P. Burrows, M. Draper, T. Garvey, P. Lebrun, K. Peach, N. Phinney, H. Schmickler, D. Schulte, and N. Toge, A Multi-TeV Linear Collider Based on CLIC Technology: CLIC Conceptual Design Report, Reports No. CERN-2012-007; SLAC-R-985; KEK-Report-2012-1; PSI-12-01; JAI-2012-001, CERN, Geneva, 2012, https://cds.cern.ch/record/1500095?ln=en.
[21] K. Fujii, C. Grojean, M. E. Peskin, T. Barklow, Y. Gao, S. Kanemura, H. D. Kim, J. List, M. Nojiri, M. Perelstein *et al.*, arXiv:1506.05992.
[22] G. Moortgat-Pick, H. Baer, M. Battaglia, G. Belanger, K. Fujii, J. Kalinowski, S. Heinemeyer, Y. Kiyo, K. Olive, F. Simon *et al.*, Eur. Phys. J. C **75**, 371 (2015).
[23] J. P. Delahaye, M. Diemoz, K. Long, B. Mansoulié, N. Pastrone, L. Rivkin, D. Schulte, A. Skrinsky, and A. Wulzer, arXiv:1901.06150.
[24] M. Boscolo, J. P. Delahaye, and M. Palmer, Rev. Accel. Sci. Techol. **10**, 189 (2019).
[25] H. Al Ali, N. Arkani-Hamed, I. Banta, S. Benevedes, D. Buttazzo, T. Cai, J. Cheng, T. Cohen, N. Craig, M. Ekhterachian *et al.*, Rep. Prog. Phys. **85**, 084201 (2022).
[26] M. Fabbrichesi, E. Gabrielli, and G. Lanfranchi, *The Physics of the Dark Photon* (Springer, New York, 2021).
[27] A. M. Sirunyan *et al.* (CMS Collaboration), Phys. Rev. Lett. **124**, 131802 (2020).
[28] J. P. Lees *et al.* (*BABAR* Collaboration), Phys. Rev. Lett. **113**, 201801 (2014).
[29] P. Ilten, Y. Soreq, J. Thaler, M. Williams, and W. Xue, Phys. Rev. Lett. **116**, 251803 (2016).
[30] R. Aaij *et al.* (LHCb Collaboration), Phys. Rev. Lett. **124**, 041801 (2020).
[31] G. Aad *et al.* (ATLAS Collaboration), Phys. Rev. D **92**, 092001 (2015).
[32] A. M. Sirunyan *et al.* (CMS Collaboration), J. High Energy Phys. 10 (2019) 139.
[33] E. Gabrielli, B. Mele, M. Raidal, and E. Venturini, Phys. Rev. D **94**, 115013 (2016).
[34] S. Biswas, E. Gabrielli, M. Heikinheimo, and B. Mele, Phys. Rev. D **93**, 093011 (2016).
[35] P. Langacker, Rev. Mod. Phys. **81**, 1199 (2009).
[36] J. Alexander, M. Battaglieri, B. Echenard, R. Essig, M. Graham, E. Izaguirre, J. Jaros, G. Krnjaic, J. Mardon, D. Morrissey *et al.*, arXiv:1608.08632.
[37] H. Davoudiasl, H. S. Lee, and W. J. Marciano, Phys. Rev. Lett. **109**, 031802 (2012).
[38] T. G. Rizzo, J. High Energy Phys. 07 (2018) 118.
[39] Z. C. Liu, C. X. Yue, and Y. C. Guo, arXiv:1703.00153.
[40] C. H. Nam, Phys. Rev. D **105**, 075015 (2022).
[41] B. Holdom, Phys. Lett. **166B**, 196 (1986).
[42] N. Arkani-Hamed and N. Weiner, J. High Energy Phys. 12 (2008) 104.
[43] M. Baumgart, C. Cheung, J. T. Ruderman, L. T. Wang, and I. Yavin, J. High Energy Phys. 04 (2009) 014.
[44] I. Hoenig, G. Samach, and D. Tucker-Smith, Phys. Rev. D **90**, 075016 (2014).
[45] J. M. Cline, G. Dupuis, Z. Liu, and W. Xue, J. High Energy Phys. 08 (2014) 131.
[46] C. Y. Chen, S. Dawson, and I. M. Lewis, Phys. Rev. D **91**, 035015 (2015).
[47] S. Dawson, P. P. Giardino, and S. Homiller, Phys. Rev. D **103**, 075016 (2021).
[48] A. Falkowski, C. Gross, and O. Lebedev, J. High Energy Phys. 05 (2015) 057.
[49] J. Blumlein and J. Brunner, Phys. Lett. B **701**, 155 (2011).
[50] S. Andreas, C. Niebuhr, and A. Ringwald, Phys. Rev. D **86**, 095019 (2012).
[51] A. Konaka, K. Imai, H. Kobayashi, A. Masaike, K. Miyake, T. Nakamura, N. Nagamine, N. Sasao, A. Enomoto, Y. Fukushima *et al.*, Phys. Rev. Lett. **57**, 659 (1986).
[52] S. Abrahamyan *et al.* (APEX Collaboration), Phys. Rev. Lett. **107**, 191804 (2011).
[53] R. Meijer Drees *et al.* (SINDRUM I Collaboration), Phys. Rev. Lett. **68**, 3845 (1992).
[54] M. D'Onofrio, O. Fischer, and Z. S. Wang, Phys. Rev. D **101**, 015020 (2020).
[55] M. Jacob and G. C. Wick, Ann. Phys. (N.Y.) **7**, 404 (1959).
[56] R. Aaij *et al.* (LHCb Collaboration), Phys. Rev. Lett. **115**, 161802 (2015).
[57] R. Aaij *et al.* (LHCb Collaboration), Phys. Rev. D **95**, 071101 (2017).
[58] A. V. Artamonov *et al.* (BNL-E949 Collaboration), Phys. Rev. D **79**, 092004 (2009).
[59] M. W. Winkler, Phys. Rev. D **99**, 015018 (2019).

[60] S. Foroughi-Abari and A. Ritz, Phys. Rev. D **102**, 035015 (2020).
[61] P. Abratenko *et al.* (MicroBooNE Collaboration), Phys. Rev. Lett. **127**, 151803 (2021).
[62] S. Cerci, D. S. Cerci, D. Lazic, G. Landsberg, F. Cerutti, M. Sabate-Gilarte, M. G. Albrow, J. Berryhill, D. R. Green, J. Hirschauer *et al.*, J. High Energy Phys. 06 (2022) 110.
[63] F. Kahlhoefer, A. Mück, S. Schulte, and P. Tunney, J. High Energy Phys. 03 (2020) 104.
[64] J. Alwall, M. Herquet, F. Maltoni, O. Mattelaer, and T. Stelzer, J. High Energy Phys. 06 (2011) 128.
[65] J. Alwall, C. Duhr, B. Fuks, O. Mattelaer, D. G. Öztürk, and C. H. Shen, Comput. Phys. Commun. **197**, 312 (2015).
[66] J. Alwall, R. Frederix, S. Frixione, V. Hirschi, F. Maltoni, O. Mattelaer, H. S. Shao, T. Stelzer, P. Torrielli, and M. Zaro, J. High Energy Phys. 07 (2014) 079.
[67] C. Degrande, C. Duhr, B. Fuks, D. Grellscheid, O. Mattelaer, and T. Reiter, Comput. Phys. Commun. **183**, 1201 (2012).
[68] T. Sjöstrand, S. Ask, J. R. Christiansen, R. Corke, N. Desai, P. Ilten, S. Mrenna, S. Prestel, C. O. Rasmussen, and P. Z. Skands, Comput. Phys. Commun. **191**, 159 (2015).
[69] J. de Favereau, C. Delaere, P. Demin, A. Giammanco, V. Lemaître, A. Mertens, and M. Selvaggi (DELPHES 3 Collaboration), J. High Energy Phys. 02 (2014) 057.
[70] V. Khachatryan *et al.* (CMS Collaboration), Eur. Phys. J. C **75**, 147 (2015).
[71] G. Aad *et al.* (ATLAS Collaboration), J. High Energy Phys. 03 (2020) 054.
[72] M. Aaboud *et al.* (ATLAS Collaboration), J. High Energy Phys. 12 (2018) 010.
[73] V. Khachatryan *et al.* (CMS Collaboration), Phys. Lett. B **760**, 448 (2016).
[74] A. Tumasyan *et al.* (CMS Collaboration), Phys. Rev. D **104**, 072001 (2021).
[75] ATLAS Collaboration, Performance assumptions based on full simulation for an upgraded ATLAS detector at a High-Luminosity LHC, Report No. ATL-PHYS-PUB-2013-009.
[76] V. Khachatryan *et al.* (CMS Collaboration), J. High Energy Phys. 04 (2015) 164.
[77] J. E. Augustin *et al.* (SLAC-SP-017 Collaboration), Phys. Rev. Lett. **33**, 1406 (1974).
[78] M. Greco, G. Pancheri-Srivastava, and Y. Srivastava, Nucl. Phys. **B171**, 118 (1980); **B197**, 543(E) (1982).
[79] M. Greco, G. Pancheri-Srivastava, and Y. Srivastava, Nucl. Phys. **B101**, 234 (1975).
[80] O. Nicrosini and L. Trentadue, Phys. Lett. B **196**, 551 (1987).
[81] R. Franceschini and M. Greco, Symmetry **13**, 851 (2021).